Dependence of the magneto-optical signal on the Co layer thickness asymmetry in Co/Pt/Co films

Ramon Weber [1,2] Carmen Martín Valderrama [1,3] Lorenzo Fallarino [1] and Andreas Berger [1]

[1]*CIC nanoGUNE BRTA, E-20018 Donostia - San Sebastián, Spain*
[2]*University of the Basque Country (UPV/EHU), E-20018 Donostia - San Sebastián, Spain*
[3]*Faculty of Science, University of Valladolid, E-47011 Valladolid, Spain*

We have studied the magneto-optical response of $Co(t_1)/Pt(d)/Co(t_2)$ trilayer structures, in which the total Co thickness $(t_1 + t_2)$ was held constant, but the split between the top and bottom layer made variable to investigate the impact of the Co layer thickness asymmetry $a_t = (t_1 - t_2)/(t_1 + t_2)$ as well as the influence of the Pt interlayer thickness d. The optical and magneto-optical properties of these films were measured using generalized magneto-optical ellipsometry. A set of specifically designed inverted double-wedge structures were characterized to determine the influence of d and especially of a_t, which should be significant if quantum-well states are relevantly modified by the Co layer thickness asymmetry. In addition to a Co/Pt interface proximity effect that leads to an overall enhancement of the magneto-optical response, we do not find the expected quadratic a_t effect, but instead observe a strong linear a_t effect. We also compare our experimental results to a classical optics description based upon the transfer matrix method, but we can achieve agreement in between these calculations and our experimental data only if we assume massively anomalous optical wave attenuation in Pt. This perceived anomalous attenuation of Pt is not observed for Co/Pt/Co trilayer structures with much thicker Co films, in which quantum-well states should not be relevant anymore. Thus, the origin of the unexpected strong linear a_t effect in ultrathin Co/Pt/Co trilayers cannot be a local materials modification, but instead must be associated with the collective nature of quantum-mechanical electronic states in asymmetric trilayers.

I. INTRODUCTION

The existence of quantum-well (QW) states in magnetic thin films and multilayers has been known and experimentally confirmed for many years, and the concept of QW states has been utilized to explain one of the most relevant phenomena in magnetism in recent history, namely the interlayer exchange-coupling effect of ferromagnets separated by nonmagnetic interlayers [1–6]. The interlayer exchange coupling between two magnetic layers was first discovered by Grünberg *et al.* in 1986 for Fe/Cr sandwich structures [7] and led to the discovery of giant magnetoresistance in 1988 [8,9]. This discovery was essential for the unprecedented advancement of modern storage technology, given that it was utilized in hard disk drives since the 1990s, and furthermore facilitated new technologies, such as nonvolatile magnetic random-access memories [10] that are commercially available today. Subsequently, insulators were also explored as interlayer materials, which can be utilized as a tunnel barrier between ferromagnetic layers, hereby increasing the resistance of devices [11] and enabling even larger areal storage densities [12]. As far as interlayer coupling itself was concerned, long- and short-period oscillations were found in a number of ferromagnetic (FM)/nonmagnetic (NM) material systems [13–18], and the periodicity could be explained by means of the Ruderman-Kittel-Kasuya-Yosida interaction as well as QW-state theoretical approaches [19–21].

Despite this long tradition of investigations focused on exchange coupling in the presence of interfaces and nontrivial multilayer structures, substantial aspects remain unclear [22]. For example, there are recent contradictory reports on paramagnetic interlayers and their ability to produce appreciable interlayer coupling even at tens of nm thickness [23–25]. As far as FM/NM interfaces in general are concerned, Pt has attracted substantial interest as NM material for a long time due to its large spin-orbit-coupling. Also, it is generally the material of choice for detection and generation of spin-currents in NM materials, due to its high spin-to-charge current conversion, which furthermore enables spin pumping [26] and the manipulation of damping [27], all aspects that are crucial for the optimization of a multitude of devices utilizing the spin degree of freedom [28]. Hereby, relevant anomalies of the spin-torque spin Hall angle were found for Co/Pt interfaces [29,30] and highlighted the premier relevance of interface quality and the associated ability of interfaces to conduct spin currents. Furthermore, spin transport phenomena like the spin Hall effect and anomalous Nernst effect are known to be modified by proximity effects [31], which also have the potential to enable new approaches to achieve electric field-controlled spintronic devices [32–35]. Thus, proximity and interface effects are a most relevant fundamental research field in modern magnetism.

In general, decreasing sizes of atomic structures such as thin films to a scale of only a few monolayers (ML) can lead to various unexpected properties of materials in comparison
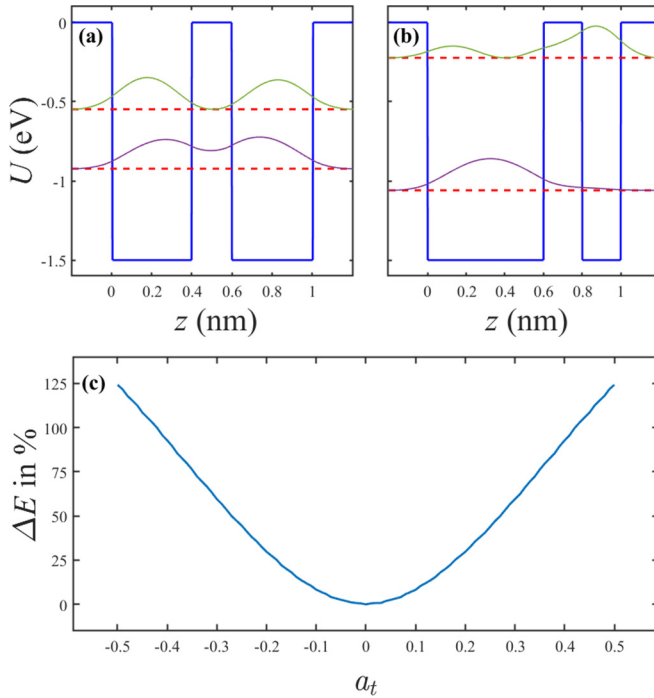
FIG. 1. Schematic of a one-dimensional quantum-mechanical double-well potential mimicking a trilayer structure having a depth profile along the z direction in its thickness symmetric (a) and asymmetric configuration (b). The schematic also displays the two lowest-lying energy levels (as dashed red lines) and associated eigenstate wave functions (as purple and green solid lines) for both cases. (c) displays the energy difference ΔE in between the two lowest-lying energy states as a function of the thickness asymmetry a_t. ΔE is hereby given in normalized units and in reference to the symmetric case $a_t = 0$, namely $\Delta E(a_t) = [\Delta e(a_t) - \Delta e(0)]/\Delta e(0)$ with $\Delta e(a_t)$ being the energy difference in absolute units.

to their common behavior in bulk dimensions. In structures in which the size of a system is reduced to the nanometer scale, surface and interface effects play an ever-increasing role, given that they constitute a large portion of the overall material. Thus, the specifics of interfacial structures in thin films or the stacking in multilayers can influence properties substantially. One such example is the recent study by Tomita *et al.* [36], which reported a significant enhancement of magneto-optical signals in thickness-modulated Fe/Pt multilayers that followed an inverse Fibonacci-like stacking order in comparison to a periodically modulated sequence while keeping the absolute thickness of each material constant. These results suggested that the magneto-optical response of a nonperiodic structure can be substantially larger than a similar periodic structure in the ultrathin limit, where quantum-mechanical (QM) interferences of electronic states such as QW states can occur.

In principle, the viability and general occurrence of these effects due to nonperiodic stacking can be understood in a simple picture with QM boundary conditions, shown in Fig. 1, in which a QM double-well potential is displayed in its thickness symmetric realization in Fig. 1(a) and an asymmetric split in Fig. 1(b). As one can clearly see, the eigenstates and their energy levels are different in both cases, and their

occurrence and values become primarily a function of the thickness asymmetry

$$a_t = \frac{t_1 - t_2}{t_1 + t_2}, \tag{1}$$

if other parameters such as the total thickness or QW depth and shape are kept constant. Hereby, t_1 and t_2 are the bottom and top layer thicknesses, respectively. Correspondingly, it is easy to understand that such an asymmetric double-well potential split will also impact the energy differences in between the QM eigenstates and accordingly optical properties, including magneto-optical properties in case of an analogous system with net spin polarization. This is illustrated in Fig. 1(c) by simply plotting the resulting relative energy difference ΔE between the two lowest energy states as a function of a_t, which exhibits a nearly parabolic behavior for our simple QM double-well potential model. Thus, we can deduce that asymmetric stacking of multilayers can indeed modify optical and magneto-optical properties, and that such an effect should be detectable already in a trilayer structure that mimics a double-layer potential, which would correspond to a FM/NM/FM layer structure with tunable a_t. The experimental exploration of this possible trilayer thickness asymmetry effect onto magneto-optical properties is the purpose of the present work.

The paper is organized as follows: in Sec. II, we define the key experimental aspects of our work, in particular the specific samples we have devised and fabricated for the purpose of our study, as well as the experimental characterization methods used. Specifically, we show how we fabricated sandwichlike ferromagnetic trilayer structures to gain insights about the influence of symmetrical vs asymmetrical ferromagnetic layer stacking onto magneto-optical effects. We document the motivation behind our choice of materials and we briefly introduce the reader to the generalized magneto-optical ellipsometry (GME) technique that enabled our quantitatively very precise magneto-optical Kerr effect (MOKE) measurements. In Sec. III, we present the results of our comprehensive experimental study and analyze them by comparing with qualitative and quantitatively accurate optical models that are based on sensible assumptions of increasing detail and in accordance with our overall experimental results. Hereby, we accomplish an accurate description of the entire set of our experimental results, from which we can derive relevant conclusions that are described in Sec. IV.

II. SAMPLES AND MEASUREMENT METHODS

As outlined in the Introduction, our aim here is to investigate if the specific stacking of layers in the thickness range, in which QM effects are relevant, will lead to a substantial modification of magneto-optical properties. Our approach is hereby to simplify the original multilayer structure utilized by Tomita *et al.* [36] by breaking down the rather complex structure to its base unit, namely a simple trilayer structure consisting of two ferromagnetic films separated by a metallic nonmagnetic interlayer, in which the ferromagnetic films represent different values of a_t. Ideally, the samples should be identical in all aspects other than a_t, such as representing a constant total thickness, for instance. Growing a sandwich structure with

two inverted wedges, as displayed in Fig. 2(a), can achieve all experimental requirements in only one sample. In fact, this approach guarantees superior reliability and reproducibility due to the inherently identical fabrication conditions, while obtaining a locally changing thickness asymmetry a_t along the full length of a single sample. Given this stacking geometry, the trilayer structure is only symmetric in the center of the sample in terms of having equal thicknesses for the top and bottom ferromagnetic Co layers. Thus, we observe along the length of the samples an increase of the absolute asymmetry towards the edge with thicker bottom (thinner top) Co layer for positive asymmetry and thicker top (thinner bottom) Co layer for negative asymmetry. Given this design, we are now able to explore the a_t space by scanning our measurement tool along the length of the sample, i.e., make point by point local measurements of the optical and magneto-optical signals, and simply vary a_t by varying the position along the sample length.

Our samples have been fabricated by means of sputter deposition using an AJA International Inc. ATC 2200-V ultrahigh-vacuum system with base pressure of better than 2×10^{-5} mTorr. Due to its rotatable sample holder and tiltable guns, this system can be easily utilized to fabricate thin films with uniform thickness as well as wedge-type structures with diverse thickness gradients along a full 4-in. wafer, or in our case here, along the length of a cut wafer segment in the form of a stripe. The desired design of the entire stack is depicted in Fig. 2(a), and the full dimensions of a typical sample with around 9-cm length are shown in a photograph in Fig. 2(b). To fabricate the relevant central Co/Pt/Co trilayer structure of our samples, we first sputtered the bottom Co wedge in a fixed azimuthal position to facilitate the wedge growth, then deposited the Pt intermediate layer (in multiples of 0.2 nm up to a maximum total thickness of 1.6 nm) as a uniform film while rotating the sample holder, and lastly sputtered the reverse Co wedge after turning the sample's azimuthal position by 180° with respect to the initial wedge deposition process. All three layers were hereby deposited at 3 mTorr Ar pressure using rf sputtering to allow for well-controlled and stable low deposition rates. The wedge shape itself is hereby facilitated by the fact that when one side of the sample was pointing towards the appropriately tilted sputter gun, the quantity of deposited material is larger on the side of the elongated sample that is closer to the gun. Hereby, one must consider that the overall shape of the film thickness within a wedge structure is not generally linear, so that this process had to be optimized to achieve a linear profile. Specifically, the inclination angle of the sputter gun was varied, and a set of test structures was fabricated. For each inclination angle of the gun, a Co wedge was grown at 25 W and its layer thickness was analyzed locally by spectroscopic ellipsometry until we observed a nearly perfectly linear profile representing an effective thickness gradient of around 22 pm thickness per millimeter in position shift x. Furthermore, we intended our samples to be constructed from individual wedges that are 1 nm thick on one side and 3 nm thick on the other end, so that we could cover a substantial a_t range. Hereby, we wanted the thicknesses of the trilayer system to be small enough so that QM effects should be visible, while not be so thin that small thickness
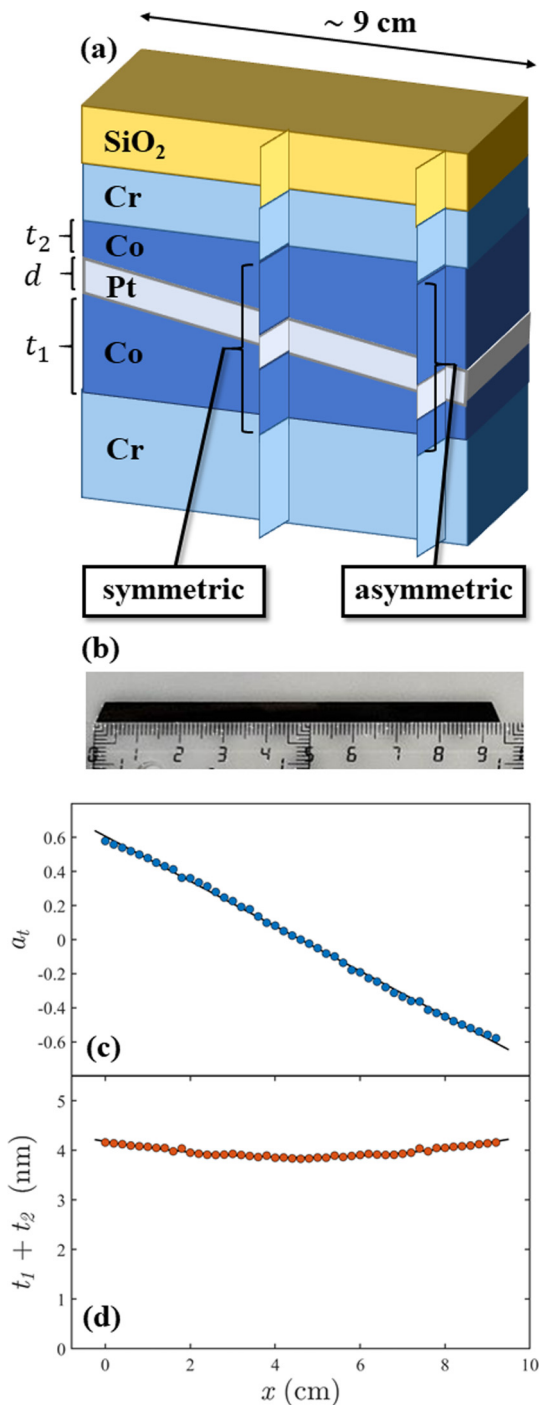

FIG. 2. Illustration of our sample structure (a) consisting of a central portion containing two inverted ferromagnetic Co wedges separated by a Pt interlayer of constant thickness, which was varied in between 0 and 1.6 nm, and outer-segment Cr films, as well as a protective Si-oxide overcoat; (b) shows a photograph of an actual sample of approximately 9-cm length; (c) experimental a_t vs lateral position data (blue dots) for one of our samples in comparison to a perfect linear relationship (black line); (d) experimentally determined total Co thickness (red dots) as a function of lateral position for the same representative sample in comparison to a least-squares fit to a parabolic function (black line).

variations would cause very significant relative sample to sample variations.

The final calibration samples also served as a calibration tool for the determination of local Co deposition rates, the determination of the experimental a_t vs position characteristic, and the absolute Co thickness t vs position check. The resulting characteristics of one of our real samples are shown in Fig. 2, where we see the change in asymmetry a_t along the sample position in (c), which is showing a nearly perfect linear trend, which was our goal. In Fig. 2(d), we see that the total Co thickness t is indeed nearly constant along the length of our samples and varies from its thinnest to its thickest portion by less than 0.4 nm. Nonetheless, these thickness variations are not random, but have a clear quadratic shape, that is the result of a remaining small nonlinearity of our wedge structures, leading to the fact that the thinnest portion of the double wedge is located in its center. To avoid that this slight shape imperfection causes any significant effect in our further studies, we selected to use only the central portion of 40-mm length for our magneto-optical experiments, in which the absolute total thickness variation of the Co layers was less than 0.09 nm or 2%. While this restriction limited the explored thickness asymmetry range of our study to $-0.3 < a_t < 0.3$, it had the advantage that we avoided the Co thickness range, in which Co/Pt interface-induced out of plane anisotropy can lead to complete or partial out of plane magnetization orientation. In such a scenario, longitudinal and polar MOKE signals might have occurred simultaneously, which would have complicated the data analysis, even if our magneto-optical detection methodology can distinguish and separate them. Instead, the thinnest Co layer as part of our Co/Pt/Co trilayer structures that we actually investigated was 1.4 nm thick, which is above the Co film-thickness range, where out of plane magnetizations occur [37].

As substrates for our samples we used (110)-oriented Si wafer strips that were covered by an approximately 3-nm-thick native SiO_2 layer. On top of the substrate, a 30-nm-thick Cr layer was deposited via DC sputtering at 80 W as an adhesion layer and to create a smooth template for our trilayer structure. As illustrated in Fig. 2(a), we covered each trilayer sample with an additional 10-nm-thick Cr film, which itself was coated by a 10-nm-thick SiO_2 layer, grown at 100 W. The Cr film was hereby utilized to guarantee that the outer Co interfaces were nominally identical, because they were both Co/Cr interfaces and thus avoided any further asymmetry effect in our structures in addition to the intended Co thickness asymmetry a_t. The additional SiO_2 overcoat was chosen to prevent oxidation and sample degradation. SiO_2 was chosen as cover material, due to its low extinction coefficient and anticorrosive properties enabling MOKE measurements with extremely high precision.

In a similar manner, we also fabricated Co/Pt/Co trilayer structures with thicker Co films to generate reference samples, in which the magnetic layer thicknesses were 5 nm or larger, and for which one would not expect QW states to be relevant anymore and affect their magneto-optical properties. The only difference in the fabrication of these reference samples in comparison to the above-described methodology was that the Co films were designed to have uniform thicknesses and the Pt interlayer was deposited in a wedgelike shape to investigate the Pt film-thickness effect using a single sample with laterally uniform Co films above and below.
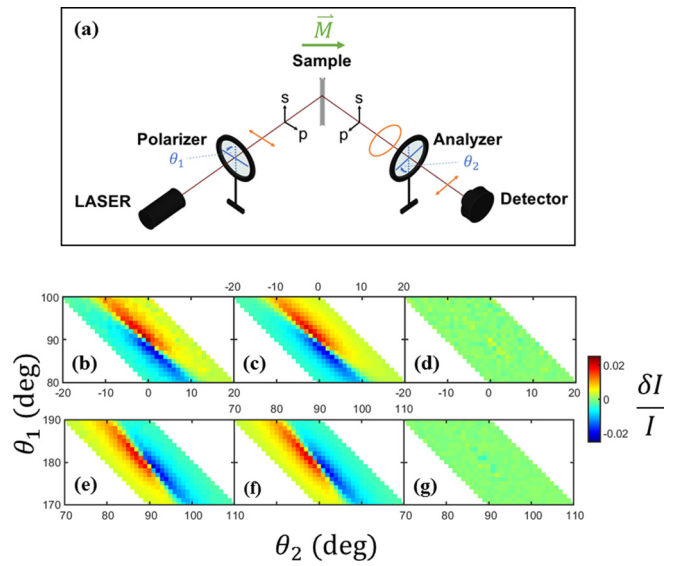

FIG. 3. (a) Schematic of our GME setup; (b) and (e) display experimental $\delta I/I(\theta_1, \theta_2)$ data as color-coded maps, measured for the same sample (a symmetric Co/Pt/Co trilayer with 0.8 nm Pt thickness) and the same applied field strength ($H = 130$ mT) in the vicinity of the s-p- and p-s-crossing-point configuration, respectively; (c) and (f) show the corresponding least-squares fit of Eq. (5) to the experimental data, which was accomplished with the same fit parameters for both experimental data sets simultaneously, representing a coefficient of determination value of $R^2 = 0.9916$; (d) and (g) display the corresponding residuals between fit and experimental data; the color code that applies to (b)–(g) is shown on the right-hand side of the figure.

Generalized magneto-optical ellipsometry was utilized to investigate the local optical and magneto-optical properties of our samples enabled by this methodology's ability to determine simultaneously the full reflection matrix and its optical and magneto-optical coefficients with high accuracy, in addition to its potential to perform vector magnetometry in only one setup [38,39]. A schematic of the experimental setup is shown in Fig. 3(a), which contains the following main elements: an ultralow-noise laser emitting at 635-nm wavelength, two linear polarizers, with one being located in the incident and one in the reflected beam path, the sample inside the gap of an electromagnet, and a photodetector to measure the reflected light intensity as a function of the applied magnetic field. In a typical measurement, the azimuthal angles θ_1 and θ_2 of the polarizers are first set to a certain combination close to extinction to be sensitive to the magneto-optical Kerr effect. Then, the magnetic field is swept to measure a full hysteresis loop and determine the normalized light intensity change at the detector, due to magnetic field and associated magnetization reversal [40] as

$$\frac{\delta I}{I}(H) = 2\frac{I(+H) - I(-H)}{I(+H) + I(-H)}. \tag{2}$$

Such measurements are then repeated for different settings of the azimuthal angles θ_1 and θ_2 of the polarizers. In our measurements here, the magnetic field is applied in the so-called longitudinal configuration, which is parallel to the

plane of our sample and the plane of incidence of the light. After having measured a series of MOKE loops for different polarizer orientations, we can obtain a map of the normalized light-intensity changes according to Eq. (2) for every applied magnetic field value. Each pixel, shown in the maps in Figs. 3(b) and 3(e), represents one of the 441 measured normalized intensity changes at the maximum applied field value for the very polarizer angle combination (θ_1, θ_2) that defines its position in the plot. The resulting signal pattern is hereby representative of the optical and magneto-optical properties of our sample, which are described by the reflection matrix $\underline{R}$, and whose determination is the goal of our GME measurements. To understand how one extracts the full reflection matrix $\underline{R}$ from such data, we need to consider that the electric field vector at the detector E_F is given by

$$E_F = \underline{P_2} \, \underline{R} \, \underline{P_1} E_I, \tag{3}$$

with $\underline{P_1}$ and $\underline{P_2}$ being the Jones matrices of the polarizers, E_I the electric field vector of the light emitted by the laser, and $\underline{R}$ the reflection matrix of the sample [38,41], given as

$$\underline{R} = r_p \begin{pmatrix} \tilde{r}_s & \tilde{\alpha} + \tilde{\gamma} \\ -\tilde{\alpha} + \tilde{\gamma} & 1 + \tilde{\beta} \end{pmatrix}, \tag{4}$$

where the complex parameters $\tilde{\alpha}$, $\tilde{\beta}$, and $\tilde{\gamma}$ describe the magneto-optical response of the longitudinal, transverse, and polar magnetization components, respectively, as well as $\tilde{r}_s = r_s/r_p$ with r_s and r_p being the purely optical Fresnel coefficients for s- and p-polarized light. Based upon this description, we can calculate the intensity at the detector $I = E_F E_F^*$, and derive an equation for the normalized intensity change $\delta I/I$ upon magnetization inversion, which is applicable for all polarizer-analyzer angle configurations (θ_1, θ_2) and any given magnetic field value:

$$\frac{\delta I}{I}(\theta_1, \theta_2) = 4 \frac{B_1 f_1 + B_2 f_2 + B_3 f_3 + B_4 f_4 + B_5 f_5 + B_6 f_6}{f_3 + B_7 f_7 + 2 B_8 f_4 + I_0}. \tag{5}$$

Here, f_1 to f_7 are known trigonometric functions of the polarizer-analyzer angles, which are documented in the literature [40], and the B_i are parameters depending on the components of the reflection matrix, specifically $B_1 = Re(\tilde{\alpha})$, $B_2 = Re(\tilde{r}_s \tilde{\alpha}^*)$, $B_3 = Re(\tilde{\beta})$, $B_4 = Re(\tilde{r}_s \tilde{\beta}^*)$, $B_5 = Re(\tilde{\gamma})$, $B_6 = Re(\tilde{r}_s \tilde{\gamma}^*)$, $B_7 = |\tilde{r}_s|^2$, and $B_8 = Re(\tilde{r}_s)$. Furthermore, I_0 is the background signal and as such it corresponds to the typically very small imperfections of the optical elements in our setup. It is worthwhile to notice that B_1 to B_6 are associated with the magneto-optical effects and B_7, B_8 with the purely optical contributions. In particular, B_1 and B_2 represent the longitudinal part of the magneto-optical response, which is the relevant effect in our measurement geometry, even if we evaluated all magneto-optical contributions in our data analysis. We now utilize Eq. (5) to fit our experimental datasets, such as the ones shown in Figs. 3(b) and 3(e), by considering B_1 to B_8 as free fit parameters, which enables the experimental determination of the full reflection matrix of Eq. (4).

One of the great advantages of GME over other magneto-optical measurement techniques is that the longitudinal, transverse, and polar MOKE all exhibit different symmetries in their signal pattern with respect to the s-p- and p-s crossing

points of the polarizer orientations (θ_1, θ_2) [41]. In particular, the longitudinal and polar effect can be unambiguously separated, if one compares the signal pattern around both crossing points simultaneously, whereas the transverse effect can be isolated easily by measuring in the vicinity of only one crossing point. Thus, to achieve extremely high precision in our experiments here, we have measured all samples using both configurations, i.e., polarizer orientations near the s-p- and the p-s-crossing points, even if we only expect a longitudinal effect to occur.

Figures 3(b) and 3(e) show such exemplary datasets, measured for the same sample and applied field, namely the symmetric Co/Pt/Co structure with 0.8 nm Pt interlayer thickness and an applied magnetic field of 1300 Oe, which saturates the sample. The color indicates the magnitude of the normalized intensity change upon magnetic state reversal at each polarizer angle configuration (θ_1, θ_2). In comparison with the experimental data in Figs. 3(b) and 3(e), Figs. 3(c) and 3(f) exhibit the corresponding least-squares fit according to Eq. (5), using the same reflection matrix and thus the same set of parameters B_1 to B_8 for both data sets. As one can see from this comparison, the fits are extremely precise and almost indistinguishable from the experimental data in accordance with the very high value for the coefficient of determination $R^2 = 0.9916$ for this typical dataset. The methodological reliability of GME is furthermore corroborated by Figs. 3(d) and 3(g), which show the residuals, i.e., the difference between the data and the fit. The residuals are essentially zero everywhere, except for some noise occurring near the diagonal of the images, which is associated with the very low overall light intensity that occurs in those regions due to the crossing of both polarizers [42]. The signal pattern that we observe and that is reproduced by the fit is characteristic for a longitudinal magneto-optical signal, and our quantitative evaluation verifies that polar and transverse MOKE contributions can be neglected for the saturated magnetization state shown here. Nonetheless, we have analyzed all MOKE components for all samples to ensure that only the longitudinal one was relevant in every case. We repeated the former measurement procedure for different positions of our stripelike samples, hereby moving the sample position in steps of 5 mm. To facilitate this, the samples were mounted on a linear translation stage to scan the position-dependent magneto-optical properties of our samples with laterally varying Co thickness asymmetry a_t.

III. RESULTS AND DISCUSSION

Using the GME methodology, we have determined the reflection matrix of all our samples and by doing so, we have quantitatively characterized the magneto-optical response for our Co/Pt/Co trilayer structures as a function of the Co thickness asymmetry a_t as well as the Pt interlayer thickness d in a very precise and reproducible manner. In Fig. 4, we present the field dependence of the relevant B_i parameters for one exemplary sample, as well as the resulting coefficient of determination R^2 representing the quality of the GME data fits to Eq. (5) for any given field. In particular, the longitudinal MOKE part is represented by B_1 and B_2 in Fig. 4(a), which are associated with the complex magneto-optical quantity $\tilde{\alpha}$ in the reflection matrix. As one can see from these data, the
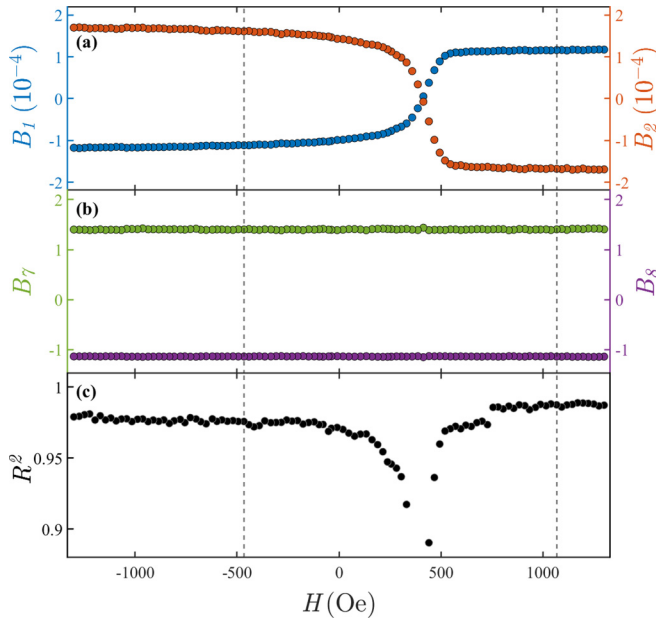
FIG. 4. Applied-field H dependence of the experimentally determined GME fit parameters, displaying the magneto-optical response B_1 (blue) and B_2 (red) in (a) and pure optical sample properties B_7 (green) and B_8 (purple) in (b); the data were measured for a symmetric Co/Pt/Co trilayer with 0.8-nm Pt thickness; (c) shows the corresponding values for the coefficient of determination R^2 of the GME data fits to Eq. (5).
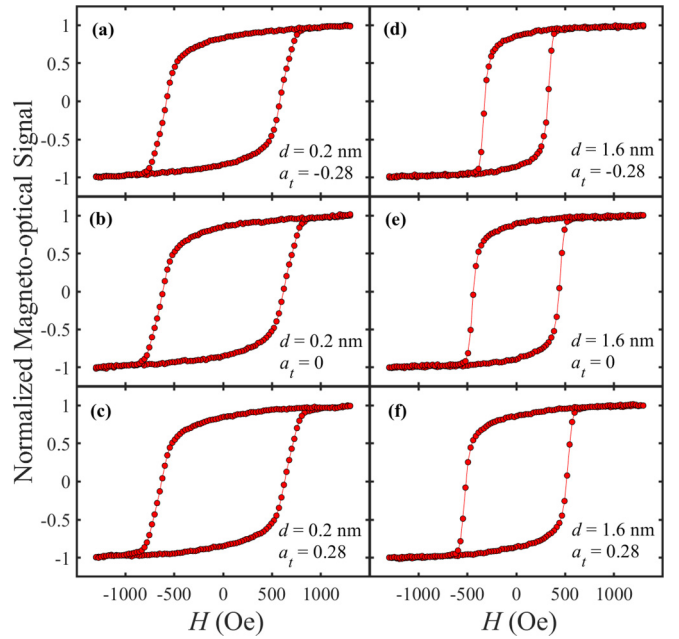

FIG. 5. Applied-field H dependence of the measured magneto-optical signal (full hysteresis loops) for six different sample configurations, namely an interlayer Pt thickness of 0.2 nm and Co layer thickness asymmetry a_t equal to -0.28 (a), 0 (b), and 0.28 (c), respectively, as well as an interlayer Pt thickness of 1.6 nm and Co layer thickness asymmetry a_t equal to -0.28 (d), 0 (e), and 0.28 (f), respectively. All magneto-optical signals are normalized to the maximum value measured for each sample.

longitudinal signal switches smoothly at the coercive field and reaches saturation quite easily along the magnetic field direction. The data suggest that both Co layers behave as if they form a single magnetic entity, which is unsurprising in this case, given that Co/Pt multilayers with 0.8-nm Pt layer thickness typically exhibit a ferromagnetic coupling throughout the multilayer stack [37]. Furthermore, Fig. 4 shows data for the case of symmetric Co thickness, which should exhibit a single magnetic reversal structure in a hysteresis loop, given that even in the absence of interlayer coupling through the Pt, the Co films on top and bottom are nominally identical.

In contrast to B_1 and B_2 in Fig. 4(a), the parameters B_7 and B_8 in Fig. 4(b) remain constant due to their purely optical nature, verifying the validity of our approach and the capability of GME to separate optical and magneto-optical parts of the reflection matrix and its associated dielectric tensor for the material under investigation. The other magneto-optical fit parameters $B_3 - B_6$ are equal to zero within their margin of error in our measurements. From the field dependence of R^2 we can see that our experimental data are very precisely reproduced by the fit to Eq. (5) everywhere, except for the immediate vicinity of the coercive field, where the magneto-optical signal becomes very small and thus relatively noisy. Given that the magneto-optical fit parameters exhibit a saturation type of behavior, meaning that they are constant over a certain magnetic field range, we can improve the accuracy of our sample characterization by averaging the B_i values over both saturation regions. The field range that we utilized for this averaging was chosen accordingly by being far away from the coercive field and requiring R^2-values to be larger than 0.97.

In Fig. 4 the utilized ranges for our averaging procedure for this particular sample are indicated by the vertical dashed lines with the data for high positive and negative fields entering our further analysis.

To ensure that we reach a stable and saturated magnetization state for all samples, we have analyzed the field dependence of the magneto-optical signal for all measurements, meaning for all Pt thickness and a_t values that we investigated. Figure 5 shows several representative examples of our measurements, in particular for structures with a thin and a thick Pt interlayer and in both of these cases for a_t values that represent the minimum and maximum of the explored parameter range, as well as $a_t = 0$. As we can see from the data, the hysteresis loops are rather conventional, and even if we do observe a d and a_t dependence of the coercivity in Fig. 5, they exhibit clearly identifiable saturation ranges, which we have utilized for the quantitative analysis of all our MOKE-signals.

Because the transverse and polar MOKE-signals are zero within their respective error bars, we will focus in the following on the longitudinal MOKE signal amplitude $|\tilde{\alpha}|$ and its dependence on the sample structure, in particular its dependence from the Co thickness asymmetry a_t. To aid the discussion of our many experimental results, we should however first estimate how $|\tilde{\alpha}|$ would change as a function of a_t if one were to assume a simple additive model for magneto-optical effects in the thin-film limit. For this, we consider that the MOKE signal generated by each Co layer increases linearly with thickness. At the same time, each Co layer

attenuates its own signal equivalent to half of its thickness to mimic the attenuation effect that the top parts of the same film have onto the signal generated by the bottom parts. In our trilayer structure, the MOKE signal coming from the top Co layer is only attenuated by itself. In contrast to that, the MOKE signal coming from the bottom Co layer is not only attenuated by itself, but also by the Pt interlayer and the top Co layer. That is the reason why we expect the absolute contribution of the magneto-optical response coming from the bottom layer to be smaller than the one of the top layer for $a_t = 0$ under the simplified conditions that we assume here. Under these assumptions, we find the total longitudinal MOKE amplitude $|\tilde{\alpha}|$ to be given as

$$|\tilde{\alpha}| = |\tilde{\alpha}|_2 + |\tilde{\alpha}|_1 = |\tilde{\alpha}|_0 \left(t_2 \left(1 - \frac{t_2}{2\delta_{Co}} \right) \right.$$
$$\left. + t_1 \left(1 - \frac{t_1}{2\delta_{Co}} \right) \left(1 - \frac{d}{\delta_{Pt}} \right) \left(1 - \frac{t_2}{\delta_{Co}} \right) \right). \quad (6)$$

Herein $|\tilde{\alpha}|_1$ represents the signal amplitude coming from the bottom Co layer, while $|\tilde{\alpha}|_2$ is related to the top Co layer, $|\tilde{\alpha}|_0$ is a constant magneto-optical factor, and δ_{Pt} and δ_{Co} are defined as the information depth of the respective material, which is proportional to the skin depth. By taking into consideration that $a_t = \frac{t_1 - t_2}{t}$, $t = t_2 + t_1$, and neglecting terms of third order in t consistent with the overall thin-film assumption, we can derive the $|\tilde{\alpha}|$ versus a_t dependency that one would expect in this simple additive thin-film limit, namely

$$|\tilde{\alpha}|(a_t) = A + Ba_t + Ca_t^2, \quad (7)$$

with

$$A = |\tilde{\alpha}|_0 \, t \left[1 - \frac{d}{2\delta_{Pt}} + t \left(\frac{3d}{8\delta_{Co}\delta_{Pt}} - \frac{1}{2\delta_{Co}} \right) \right], \quad (8)$$

$$B = -|\tilde{\alpha}|_0 \, t \left[\frac{d}{2\delta_{Pt}} - t \frac{d}{4\delta_{Co}\delta_{Pt}} \right], \quad (9)$$

$$C = -|\tilde{\alpha}|_0 \cdot \frac{d \cdot t^2}{8\delta_{Co}\delta_{Pt}}. \quad (10)$$

Within this simple picture, one would expect a parabolic $|\tilde{\alpha}|$ versus a_t dependence, in which the coefficients are only determined by the Pt interlayer thickness d, the information depths of the materials, and the total Co thickness t. Furthermore, we should expect all derived parameters to decrease monotonically with the Pt interlayer thickness. The thicker the interlayer, the stronger the signal is attenuated with increasing a_t as represented by parameter B. As our approximation shows, also parameters A and C should be decreasing slightly with the Pt thickness, while the attenuation parameter B and the second-order parameter C should be zero without any Pt interlayer. With this in mind, we are now ready to discuss our experimental results. Given the definition of the B_i, we determined the longitudinal Kerr amplitude from our experimental data via

$$|\tilde{\alpha}| = \sqrt{B_1^2 + \left(\frac{B_2 - B_1 B_8}{\sqrt{B_7 - B_8^2}} \right)^2}. \quad (11)$$
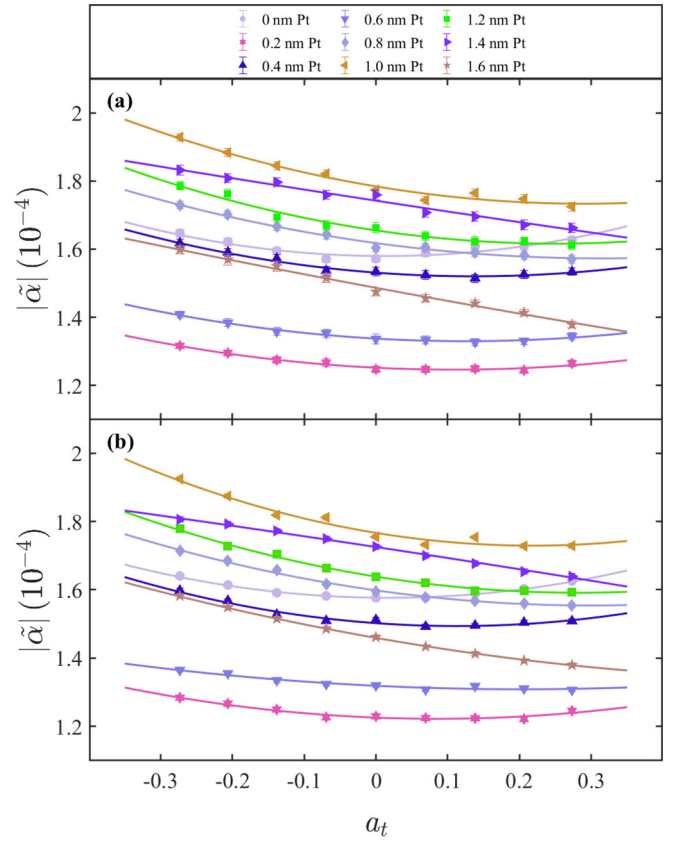

FIG. 6. Experimentally determined longitudinal Kerr effect amplitude values $|\tilde{\alpha}|$ vs Co layer thickness asymmetry a_t measured in the positive (a) and negative (b) saturation regions that are defined in Fig. 4. The symbols show experimental data with each color representing a different Pt interlayer thickness that is defined in the legend, while the solid lines of equal color represent least-squares fits to Eq. (7). The error bars are only partially visible, because they are smaller than the data symbols for most data points.

The resulting experimental datasets are displayed in Figs. 6(a) and 6(b) as a function of a_t for both saturation conditions, which we defined exemplary in Fig. 4. The different colors of the data points correspond to samples with different Pt interlayer thickness, and the respective lines represent least-squares fits of Eq. (7) to the datasets for constant Pt thickness by using A, B, and C as free fit parameters. First, we notice that the overall signal amplitude changes relevantly with the Pt thickness. This is the most pronounced effect that we observe in our data and it is independent from the Co thickness asymmetry a_t. Furthermore, this shift is nonmonotonous, so that the datasets corresponding to the different Pt thicknesses move up and down in Fig. 6. Secondly, we detect a modest change in $|\tilde{\alpha}|$ with asymmetry a_t for all samples. While this variation is rather minor and mostly quadratic for the pure Co sample, an additional linear contribution occurs for increasing Pt thickness. We can also see by comparing Figs. 6(a) and 6(b) that both datasets are consistent and show the same sample behavior qualitatively and quantitatively. It is furthermore important to notice that all datasets are extremely well represented by Eq. (7), at least as long as one considers A, B, and C to be free parameters. Thus, we can utilize these

parameters for our further discussion and our attempt to devise a fully quantitative model and complete understanding of all our data.

The experimentally determined parameter values are shown in Fig. 7 as a function of the Pt layer thickness d for positive (dots) and negative (circles) saturation fields, respectively. In contradiction to Eq. (10) of our qualitative model, we find a nonvanishing positive C parameter describing the quadratic a_t dependency of the magneto-optical signal even without a Pt interlayer being present in our samples, depicted in Fig. 7(a). By adding Pt to the structure, this second-order contribution does not change significantly, and accordingly we cannot identify the experimentally observed quadratic a_t effect as being representative of a true quadratic asymmetry effect. Instead, it must be related to still existing minor total Co thickness variations in the sample, which will cause a total signal variation and exhibit a quadratic characteristic. This is consistent with the quadratic total thickness dependence that we observed in Fig. 2(d), which is the result of a slight nonlinearity of the wedge shape. The thickness variations are very small, but our very sensitive GME measurements allow us to detect them. The fact that C is nearly independent from the Pt thickness now means that there is no noticeable true quadratic thickness asymmetry effect in any of our samples, and instead the perceived parabolic a_t dependence is induced by the slight parabolic t dependence for all our samples.

The B-parameter results in Fig. 7(b) exhibit a zero value without Pt interlayer and follow a decreasing trend with growing Pt interlayer thickness, qualitatively consistent with the predicted falloff in Eq. (9) and thus, they seem to be representative of the extinction caused by the Pt interlayer. Parameter A, which represents the MOKE amplitude for the symmetric case, shows a complicated behavior and specifically is not decreasing in a monotonous fashion as one would have expected from Eq. (8). While we find a general decline of A with Pt thickness, we observe a superimposed upward shift of the data in the thickness range in between 0.6 and 1.0 nm Pt thickness, in contrast to our qualitative expectations according to Eq. (8).

To properly verify the above observations based upon our qualitative model, we calculated the quantitative response of our structures by an exact classical model of magneto-optical effects by using the transfer-matrix approach of Schubert [43]. For this, we did not only take the Co and Pt layers into consideration, but also the Si substrate, as well as the Cr and SiO$_2$ layers. Hereby, we developed a sequence of model assumptions of increasing refinement to achieve a full quantitative description of our experimental results. Each of these models consists of the full layer stack of our samples, but only the Co/Pt/Co trilayer structure was modified in its optical and magneto-optical properties according to the schematics displayed in Fig. 7(d). Furthermore, these models also took into account the already-mentioned small Co layer thickness variations along the length of the wedge that led to nonvanishing C-parameter values even in the case without Pt interlayer. The specific formalism for our simulations is described in the Appendix, which also provides information about all optical constants we used and which were identical for all materials in all of our models, as given in Table I, except for Pt, which we had to vary as will be discussed in the following. In our computations the full reflection matrix is obtained for each
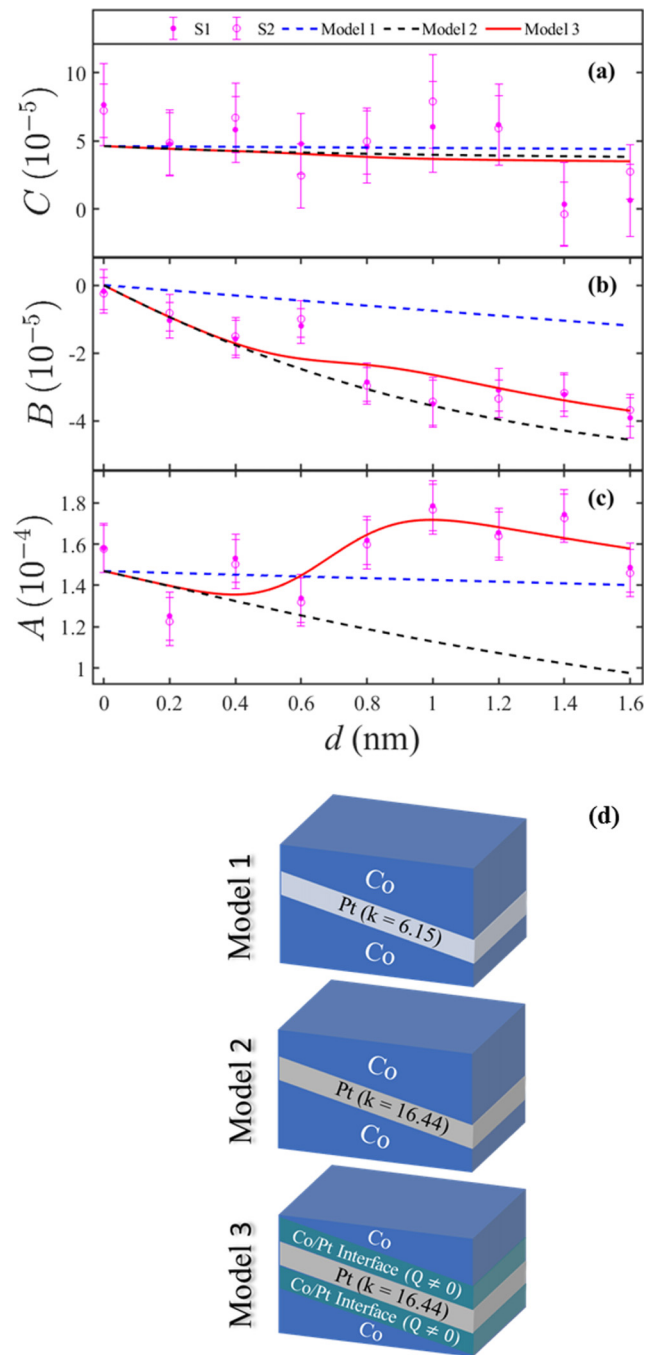

FIG. 7. Pt thickness d dependence of the Co thickness asymmetry a_t effects onto the magneto-optical signal, represented by a quadratic term C (a), a linear term B (b), and a constant term A (c), according to Eq. (7). The measured data are shown for both saturation regions S1 (positive) and S2 (negative), which were defined in Fig. 4, while the lines represent results of calculations for the three optical models displayed in (d). While the optical models encompass the entire sample structure shown in Fig. 2(a), only the central Co/Pt/Co trilayer portion is shown in (d), given that only this portion is varied in between the models. Model 1 uses bulk optical constants only, model 2 considers the Pt interlayer to be anomalously absorptive, and model 3 furthermore introduces magneto-optically active interface layers of finite thickness (0.3 nm) upon reaching a Pt layer thickness threshold of 0.7 nm. All optical and magneto-optical parameters utilized in the model calculations are listed in Table I.

TABLE I. Optical and magneto-optical parameters that have been applied to perform quantitative computations according to the full stack in Fig. 2(a) and varying parameters of the models as illustrated in Fig. 6(d).

Material	Refractive index n	Extinction constant k	Voigt parameter
Cr	3.1357	3.3171	
Co	2.5658	3.4725	$0.033 - 0.018\,i$
Co/Pt interface	0.46794	16.44	$0.129 - 0.070\,i$
Pt high k	0.46794	16.44	
Pt	0.46794	6.1548	
SiO$_2$	1.4636	0.0016569	
Si	3.8787	0.019221	

model and underlying specific geometry, and subsequently values for $|\tilde{\alpha}|$ vs a_t are extracted in order to determine the magneto-optical response of the structure and compute parameters A, B, and C for a comparison with our experimental data. In addition, the previously calibrated thicknesses of the layers are included in all computations as well as an incident angle of 45° for the 635-nm wavelength light to mimic the exact geometry of our experimental setup.

In our first approach, shown in Fig. 7(d), we simulate the full structure with magneto-optical constants known from literature [44–46] and a bulk Co reference sample. These results, representing model 1, are depicted in Figs. 7(a)–7(c) as blue dashed lines. Due to the earlier discussed small thickness variation within each double-wedged sample, the C parameter for all models appears upward shifted by a supplementary constant if compared to a perfect sample with truly constant t. Hence, C is the sum of two parts $C = C_1 + C_2$, with C_1 being the real asymmetry-induced effect that is quadratic in a_t, while the second part C_2 is caused by the position-dependent total thickness t. As discussed earlier, the data show an almost constant C value that is dominated by the thickness variation, whereas the classical true quadratic a_t effect is very small in comparison. Also, we see that our experimental data and the model results for C are in very good agreement, so that we cannot detect any quadratic a_t effect that would have to be ascribed to a quantum-mechanical effect based on the modification of magneto-optical properties due to the thickness asymmetry of the bilayer stacking. In contrast to model 1 explaining the data for C, we can see from Fig. 7(b) that this model cannot explain the observed linear asymmetry term, characterized by parameter B, and its Pt thickness dependence. The model predicted Pt extinction that leads to the linear $|\tilde{\alpha}|$ vs a_t dependence is far smaller than what we observe experimentally. Furthermore, this simple model 1 does not reproduce the rather complex and nonmonotonous A vs d behavior that we observe experimentally, which can be seen from a comparison of our data with the model results in Fig. 7(c). Thus, to quantitatively describe our results, we have to modify our model to incorporate modifications of optical properties that are representative of the effect of multilayer stacking in our sample and cannot be accommodated by classical local optics of bulk materials with conventional optical material constants.

Specifically, it is the conventional optical extinction of Pt that cannot explain the strong drop of the B parameter as the Pt thickness increases. Consequently, according to the classical picture of Eq. (9) the signal attenuation length of Pt has to be much smaller than for bulk Pt, which in other words means that the optical damping constant k representing the imaginary part of the complex index of refraction $N = n + ik$ appears to be anomalously high in our structures. Correspondingly, we adapted a new version of our model, identified as model 2 in Fig. 7(d), to our experimental findings to be able to mimic the attenuation of the magneto-optical response in our samples by means of an anomalously large extinction coefficient $k_{Pt} = 16.44$ for our Pt interlayer films. By assuming this artificially high k_{Pt}, which is equivalent to a skin depth of only 6 nm in contrast to the literature value of 16 nm for $\lambda = 635$ nm in accordance with the standard bulk $k_{Pt} = 6.15$ [44], model 2 achieves a much better agreement with our data as can be seen by the dashed black lines in Fig. 7. In particular, the experimentally observed strong decrease of B with d is now much better described by model 2 and in good agreement with the experimental data. Also, the C vs d dependence that was already well described by model 1 is not relevantly altered by model 2, so that it can describe overall the experimental data for B and C very well. Model 2, however, does not properly describe the A vs d dependence that we find experimentally, even if the agreement up to 0.6-nm thickness is actually very good. Specifically, the nonmonotonic upward shift of the data in the range in between 0.6 and 1.0 nm Pt thickness cannot be reproduced by our classical equivalency picture of making Pt highly absorptive, and a further refinement of our model assumptions is needed. The observed experimental behavior can, however, be understood in a rather straightforward manner, if one recalls that in Co/Pt multilayer structures, the ferromagnetic spin polarization of Co leads to a relevant proximity-induced spin polarization in the Pt interface layer, whereas Pt layers further away from the interface do not exhibit any relevant spin polarization, a fact that has been experimentally demonstrated and theoretically confirmed [47]. This proximity-induced spin polarization in the Pt layer adjacent to the Co can now generate a relevant enhancement of the total magneto-optical activity, because the Pt spin polarization in conjunction with the strong spin-orbit coupling of Pt will lead to an additional magneto-optical activity of a Co/Pt interface [48].

In order to mimic the Pt-thickness induced enhancement of the magneto-optical response around 0.7-nm Pt thickness, which leads to the nonmonotonous behavior of A in Fig. 7(c), we need to include the above-mentioned magnetic proximity effect in our model, which is associated with the Co/Pt-interfaces. Thus, in model 3 we introduce two Co/Pt interface regions between the ferromagnetic Co layers and the Pt interlayer, and we assume these interface regions to produce a substantially enhanced magneto-optical contribution, once the quantum-mechanically determined electronic states at the interfaces are fully formed, which we consider to occur at a Pt thickness of 0.7 nm. Given local variations of the Pt interlayer thickness, we assume that the additional interface magneto-optical activity Q is not a truly abrupt function of the average layer thickness, but a slightly smeared out step function in the thickness range of 0.4 – 1.0 nm. Nonetheless,

the data in Fig. 7(c) demonstrate that the onset is sharp with no Co/Pt interface signal truly apparent at 0.6 nm Pt thickness, while being fully established for 1.0 nm, i.e., length scales that are quite typical for quantum-well states in metallic materials.

Furthermore, model 3 assumes that only a 0.3-nm-thick interface region contributes to the interface signal, while additionally added Pt does not produce any further magneto-optical signal response, consistent with prior observations that the proximity-induced spin polarization and associated enhanced spin-orbit coupling effects are limited to the Pt interface layer only [24,47]. We also keep the assumption of model 2 that the entire Pt layer exhibits an anomalously high extinction coefficient of $k_{Pt} = 16.44$. The resulting values of A, B, and C vs d for model 3 are shown as red lines in Fig. 7. As intended, model 3 is now able to reproduce the nonmonotonic behavior of A vs d, because the added interface region signal occurs in the thickness range of $0.4 - 1.0$ nm and is superimposed onto the general decline of the overall magneto-optical signal as d increases. The introduction of the interfacial regions by means of model 3 has virtually no impact on C, depicted in Fig. 7(a), so that model 3 also explains the C vs d behavior with good quantitative accuracy. The B vs d dependency for model 3 in Fig. 7(b) shows a visible modification in comparison to model 2. However, the simulated curve for model 3 is in very good agreement with our experimental data for the chosen material parameters, which were indeed selected to optimize the match of model 3 to our experimental data for all of our extracted parameters, i.e., the entirety of our A, B, and C vs d data.

Overall, we can describe our experimental results using a classical description, and for that we needed to add two modifications to the classical local optics description with bulk materials constants. One is the additional magneto-optical signal of Co/Pt interfaces, which is an unsurprising modification given that the proximity to ferromagnetic Co results in the occurrence of static spin polarization in Pt interface atoms that combined with the large spin-orbit coupling of Pt produces an added magneto-optical interface signal once the interfaces and their quantum-mechanical interface states are formed. This leads to the observed Pt thickness dependence of A and is an effect that has nothing to do with the Co layer thickness asymmetry a_t. From the C vs d dependence that we observe experimentally, we have to deduce that there is no significant quadratic a_t effect in our samples, which would be the magneto-optical equivalent of the asymmetry-induced changes in the simple QM picture of the double-well potential of Fig. 1(c). While the observed values of C are significantly different from zero, they are small and more importantly, they do not show any relevant dependency from d, so that even for $d = 0$, which is formally a simple Co film and not a trilayer structure, C is not zero due to very small, but detectable thickness variations along the elongated sample axis. However, we do observe a very strong linear signal dependence from a_t in our structures, which we did not expect. This linear a_t effect does show the proper d dependence by vanishing for $d = 0$, which is the simple Co film geometry. Upon increasing d, this linear a_t effect, represented by B, becomes large very quickly, which is inconsistent with a classical optical picture using conventional materials constants for Pt and Co. Formally, we are able to reconcile our experimental results with a classical
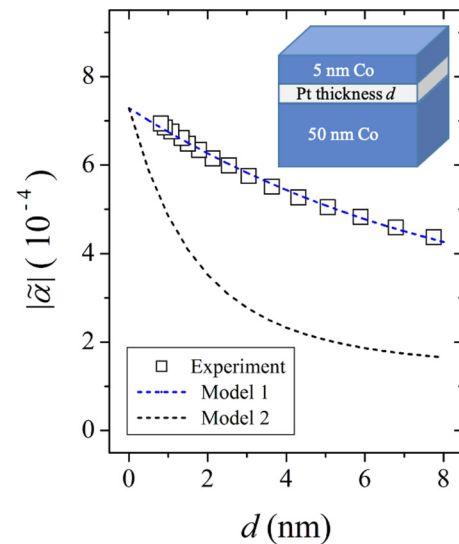

FIG. 8. Experimentally determined longitudinal Kerr effect amplitude values $|\tilde{\alpha}|$ vs Pt interlayer thickness d for a Co/Pt/Co trilayer structure with thick Co layers (the trilayer structure is schematically shown as an inset). The symbols show experimental data, while the dashed lines show the results of classical optics calculations, assuming conventional Pt properties (blue, consistent with the material constants of model 1) as well as highly absorptive Pt (black, consistent with the material constants of model 2).

optics picture, but we have to assume an anomalously high optical damping in Pt. However, this does not necessarily mean that we observe a structure-induced modification of local optical properties. It is just as possible that we observe directly a linear a_t effect that has a collective and nonlocal QM origin and is associated with the reduced symmetry of the structure once a_t deviates from zero. To be able to distinguish these two interpretations, we have also investigated a series of samples, in which the Co layer thickness was far larger, so that QW states should not impact their properties and thus any a_t dependence ought to disappear. On the other hand, these thicker film structures have the same Co/Pt interface structures, not just nominally, but also in terms of their real structure, because these samples were fabricated in the exact same way. Thus, an interface-induced local property modification should occur in such structures as well.

Figure 8 shows the experimentally determined total longitudinal MOKE amplitude $|\tilde{\alpha}|$ for Co/Pt/Co trilayer structures with thick Co films as a function of the Pt interlayer thickness d in comparison to the theoretically expected results assuming conventional Pt properties as well as highly absorptive Pt parameters. As we can see from the data alone, the signal decreases over a rather wide Pt thickness range and it is also fully compatible with model predictions using literature values for the material constants of Pt. In contrast, the highly absorptive Pt that allowed us to model the thin trilayer structures in Fig. 7 does not at all describe the observed experimental behavior in Fig. 8, but would have led to a far more rapid $|\tilde{\alpha}|$ vs d falloff. Thus, the interface-induced modification of optical properties can be excluded as an explanation for our observations, because it should have shown up in both types of structures, given that the relevant atomistic interfaces are

identical. The difference, though, is the Co film thickness and thus the expected relevance of QW states in very thin Co/Pt/Co trilayers. Therefore, our results in Fig. 7 and the contrast to the observations in Fig. 8 indicate a quantum-mechanical modification of the magneto-optical properties for sufficiently thin Co/Pt/Co trilayer structures as the result of their specific stacking structure, representing a genuine non-local stacking-asymmetry effect that is linear in a_t.

IV. CONCLUSIONS

In our study we have grown Co/Pt/Co sandwich structures with varying Co and Pt thicknesses to investigate the influence of thickness modulations in ferromagnetic multilayers and their associated QW-state modifications onto magneto-optical signal amplitudes. For this, we designed and fabricated an inverted double-wedge structure, so that within a series of a few samples, the parameter space of Pt interlayer thickness d and Co layer thickness asymmetry a_t could be robustly and reproducibly explored. Furthermore, we utilized GME to allow for extremely precise absolute MOKE measurements. In addition, we devised a series of optical models that allowed us to achieve a detailed quantitative analysis and interpretation of our data.

Upon increasing the Pt interlayer thickness of the ferromagnetic sandwich structure, we observe a relevant enhancement of the magneto-optical response of the multilayer in the Pt thickness range in between 0.6 and 1.0 nm, which is explained by the formation of magneto-optically active interfaces. This is a well-known effect for Co/Pt interfaces and it is associated with the proximity-induced spin polarization of Pt in conjunction with its strong spin-orbit coupling [47], and the previously observed thickness dependence of this interface state and signal formation matches our observation here.

More relevantly, our experimental results show unambiguously that there are indeed clear signal modifications as the Co/Pt/Co layer structure is made asymmetric. However, the signal modification did not have the type of quadratic behavior that we anticipated according to the simple QM picture of Fig. 1(c), and the modifications were also significantly smaller than what one could have expected to find based on the earlier observations by Tomita *et al.* [36]. Nonetheless, we did observe a very significant linear asymmetry effect, whose origin is more difficult to understand. By means of modeling, we could map our experimental findings onto a classical equivalency model of having an extremely absorptive Pt layer in our Co/Pt/Co trilayer structure, but such an interface-induced local optical property modification is not the true origin of the observed behavior. We could demonstrate this clearly by analyzing the magneto-optical properties of thicker trilayer structures that contain the same interface configurations, but which did not show any anomalous behavior, and instead were fully compatible with conventional optical properties for Pt. From these comparative studies, we concluded that for sufficiently thin Co/Pt/Co trilayers there is an actual linear a_t effect that has a collective and nonlocal QM origin and is associated with the reduced symmetry of the structure once a_t deviates from zero. It would be valuable to investigate the occurrence of such linear asymmetry effects for other material systems. Moreover, it would be relevant

to develop a theoretical understanding of how the lack of symmetry generates this directional effect, which appears to be somewhat analogous to the way the Dzyaloshinskii-Moriya interaction impacts exchange coupling and associated magnetization states in systems with reduced symmetry, including asymmetric multilayer structures [49,50]. Such an additional spin-orbit mechanism or channel would be prohibited in symmetric structures, but should be active in nonsymmetric ones, such as our $a_t \neq 0$ samples. Moreover, it could lead to an inequality of states that would otherwise be equivalent in their properties if this mechanism were absent. For this, a review of the underlying theoretical concepts of magneto-optical effects in the presence of asymmetric layer and magnetization structures would be important and will hopefully be triggered by our experimental observations.

APPENDIX

We performed our simulations by defining the dielectric tensor for each layer in our structure and applying the transfer matrix approach for homogeneous media [43]. In this approach, the electromagnetic response is calculated through the partial transfer matrices T_p by the in-plane field vector

$$\psi(z + d) = \exp\left(i\frac{\omega}{c}\Delta d\right)\psi(z) = T_p\psi(z), \quad (A1)$$

with z being the Cartesian coordinate related to the depth of the sample, d the layer thickness, ω the angular frequency, c the vacuum velocity of light, and Δ the wave transfer matrix. The complete transfer matrix of the multilayer is defined as

$$T = T_i\left(\prod_{j=1}^{N} T_{p,j}(d)\right)T_f, \quad (A2)$$

with T_i and T_f being the incident and exit matrix, respectively, and $T_{p,j}$ representing the partial transfer matrix of each media layer j, which can be expressed by a finite Taylor expansion. Finally, the parameters of the finite series expansion are calculated by the eigenvalues of the matrix Δ

$$\Delta = \begin{pmatrix} -k_x\frac{\epsilon_{31}}{\epsilon_0} & -k_x\frac{\epsilon_{32}}{\epsilon_0} & 0 & 1-\frac{k_x^2}{\epsilon_0} \\ 0 & 0 & -1 & 0 \\ \epsilon_{23}\frac{\epsilon_{31}}{\epsilon_0}-\epsilon_{21} & k_x^2-\epsilon_{22}+\epsilon_{23}\frac{\epsilon_{32}}{\epsilon_0} & 0 & k_x\frac{\epsilon_{23}}{\epsilon_0} \\ \epsilon_0-\epsilon_{13}\frac{\epsilon_{31}}{\epsilon_0} & \epsilon_{12}-\epsilon_{13}\frac{\epsilon_{32}}{\epsilon_0} & 0 & -k_x\frac{\epsilon_{13}}{\epsilon_0} \end{pmatrix}, \quad (A3)$$

with k_x the component of the incident wave vector parallel to the surface of the sample in the plane of incidence and ϵ_{ij} the

dielectric tensor elements defined by

$$\epsilon = \begin{pmatrix} \epsilon_0 & m_z Q \epsilon_0 & m_y Q \epsilon_0 \\ -m_z Q \epsilon_0 & \epsilon_0 & m_x Q \epsilon_0 \\ -m_y Q \epsilon_0 & -m_x Q \epsilon_0 & \epsilon_0 \end{pmatrix}. \qquad \text{(A4)}$$

Here the magneto-optical coupling constant Q is defined as $Q = Q_r - iQ_i$ [43,51]. Furthermore, we obtain the 2×2

reflection matrix $\underline{R}$ by converting the 4×4 transfer matrix in the following way:

$$\underline{R} = r_p \begin{pmatrix} \tilde{r}_s & \tilde{\alpha} + \tilde{\gamma} \\ -\tilde{\alpha} + \tilde{\gamma} & 1 + \tilde{\beta} \end{pmatrix} = \begin{pmatrix} \frac{T_{11}T_{43} - T_{41}T_{13}}{T_{11}T_{33} - T_{13}T_{31}} & \frac{T_{11}T_{23} - T_{13}T_{21}}{T_{11}T_{33} - T_{13}T_{31}} \\ \frac{T_{41}T_{33} - T_{43}T_{31}}{T_{11}T_{33} - T_{13}T_{31}} & \frac{T_{21}T_{33} - T_{13}T_{31}}{T_{11}T_{33} - T_{13}T_{31}} \end{pmatrix}.$$

$$\text{(A5)}$$

[1] J. E. Ortega and F. J. Himpsel, Phys. Rev. Lett. **69**, 844 (1992).

[2] C. Carbone, E. Vescovo, O. Rader, W. Gudat, and W. Eberhardt, Phys. Rev. Lett. **71**, 2805 (1993).

[3] M. C. Munoz and J. L. Perez-Díaz, Phys. Rev. Lett. **72**, 2482 (1994).

[4] J. E. Ortega, F. J. Himpsel, G. J. Mankey, and R. F. Willis, Surf. Rev. Lett. **04**, 361 (1997).

[5] S. S. P. Parkin, N. More, and K. P. Roche, Phys. Rev. Lett. **64**, 2304 (1990).

[6] J. E. Mattson, C. H. Sowers, A. Berger, and S. D. Bader, Phys. Rev. Lett. **68**, 3252 (1992).

[7] P. Grünberg, R. Schreiber, Y. Pang, M. B. Brodsky, and H. Sowers, Phys. Rev. Lett. **57**, 2442 (1986).

[8] G. Binasch, P. Grünberg, F. Saurenbach, and W. Zinn, Phys. Rev. B **39**, 4828 (1989).

[9] M. N. Baibich, J. M. Broto, A. Fert, F. Nguyen Van Dau, F. Petroff, P. Etienne, G. Creuzet, A. Friederich, and J. Chazelas, Phys. Rev. Lett. **61**, 2472 (1988).

[10] S. Tehrani, J. M. Slaughter, E. Chen, M. Durlam, J. Shi, and M. DeHerren, IEEE Trans. Magn. **35**, 2814 (1999).

[11] J. S. Moodera, L. R. Kinder, T. M. Wong, and R. Meservey, Phys. Rev. Lett. **74**, 3273 (1995).

[12] S. Mao *et al.*, IEEE Trans. Magn. **42**, 97 (2006).

[13] J. Unguris, R. J. Celotta, and D. T. Pierce, Phys. Rev. Lett. **67**, 140 (1991).

[14] S. T. Purcell, W. Folkerts, M. T. Johnson, N. W. E. McGee, K. Jager, J. aan de Stegge, W. B. Zeper, W. Hoving, and P. Grünberg, Phys. Rev. Lett. **67**, 903 (1991).

[15] M. T. Johnson, S. T. Purcell, N. W. E. McGee, R. Coehoorn, J. aan de Stegge, and W. Hoving, Phys. Rev. Lett. **68**, 2688 (1992).

[16] A. Fuss, S. Demokritov, P. Grünberg, and W. Zinn, J. Magn. Magn. Mater. **103**, L221 (1992).

[17] Z. Q. Qiu, J. Pearson, A. Berger, and S. D. Bader, Phys. Rev. Lett. **68**, 1398 (1992).

[18] Z. Q. Qiu, J. Pearson, and S. D. Bader, Phys. Rev. B **46**, 8659(R) (1992).

[19] M. van Schilfgaarde and W. A. Harrison, Phys. Rev. Lett. **71**, 3870 (1993).

[20] B. A. Jones and C. B. Hanna, Phys. Rev. Lett. **71**, 4253 (1993).

[21] P. Bruno, Europhys. Lett. **23**, 615 (1993).

[22] M. Li, W. Cui, J. Yu, Z. Dai, Z. Wang, F. Katmis, W. Guo, and J. Moodera, Phys. Rev. B **91**, 014427 (2015).

[23] F. Magnus, M. E. Brooks-Bartlett, R. Moubah, R. A. Procter, G. Andersson, T. P. A. Hase, S. T. Banks, and B. Hjörvarsson, Nat. Commun. **7**, 11931 (2016).

[24] L. Fallarino, B. J. Kirby, M. Pancaldi, P. Riego, A. L. Balk, C. W. Miller, P. Vavassori, and A. Berger, Phys. Rev. B **95**, 134445 (2017).

[25] L. Fallarino, P. Riego, B. J. Kirby, C. W. Miller, and A. Berger, Materials **11**, 251 (2018).

[26] H. Yang, J. Li, and W. E. Bailey, Appl. Phys. Lett. **108**, 242404 (2016).

[27] M. Caminale, A. Ghosh, S. Auffret, U. Ebels, K. Ollefs, F. Wilhelm, A. Rogalev, and W. E. Bailey, Phys. Rev. B **94**, 014414 (2016).

[28] R. Weber, D.-S. Han, I. Boventer, R. Lebrun, G. Jakob, and M. Kläui, J. Phys. D: Appl. Phys. **52**, 325001 (2019).

[29] W. Zhang, W. Han, X. Jiang *et al.*, Nat. Phys. **11**, 496 (2015).

[30] K. Garello, I. Miron, C. Avci, F. Freimuth, Y. Mokrousov, S. Blügel, S. Auffret, O. Boulle, G. Gaudin, and P. Gambardella, Nat. Nanotechnol. **8**, 587 (2013).

[31] D.-O. Kim, K. M. Song, Y. Choi, B.-C. Min, J.-S. Kim, J. W. Choi, and D. R. Lee, Sci. Rep. **6**, 25391 (2016).

[32] Y. Hibino, T. Koyama, A. Obinata, K. Miwa, S. Ono, and D. Chiba, Appl. Phys. Express **8**, 113002 (2015).

[33] A. Obinata, Y. Hibino, D. Hayakawa, T. Koyama, K. Miwa, S. Ono, and D. Chiba, Sci. Rep. **5**, 14303 (2015).

[34] K. T. Yamada, M. Suzuki, A.-M. Pradipto, T. Koyama, S. Kim, K.-J. Kim, S. Ono, T. Taniguchi, H. Mizuno, F. Ando, K. Oda, H. Kakizakai, T. Moriyama, K. Nakamura, D. Chiba, and T. Ono, Phys. Rev. Lett. **120**, 157203 (2018).

[35] S. Manipatruni, D. E. Nikonov, C.-C. Lin, T. A. Gosavi, H. Liu, B. Prasad, Y.-L. Huang, E. Bonturim, R. Ramesh, and I. A. Young, Nature (London) **565**, 35 (2019).

[36] S. Tomita, T. Suwa, P. Riego, A. Berger, N. Hosoito, and H. Yanagi, Phys. Rev. Appl. **11**, 064010 (2019).

[37] O. Hellwig, A. Berger, J. B. Kortright, and E. E. Fullerton, J. Magn. Magn. Mater. **319**, 13 (2007).

[38] A. Berger and M. R. Pufall, Appl. Phys. Lett. **71**, 965 (1997).

[39] A. Berger and M. R. Pufall, J. Appl. Phys. **85**, 4583 (1999).

[40] J. A. Arregi, J. B. González-Díaz, O. Idigoras, and A. Berger, Phys. Rev. B **92**, 184405 (2015).

[41] P. Riego, Magneto-optical characterization of magnetic thin films and interface structures, Ph.D. thesis, University of the Basque Country (UPV/EHU), 2019.

[42] J. A. Arregi, P. Riego, and A. Berger, J. Phys. D: Appl. Phys. **50**, 03LT01 (2017).

[43] M. Schubert, Phys. Rev. B **53**, 4265 (1996).

[44] W. S. M. Werner, K. Glantschnig, and C. Ambrosch-Draxl, J. Phys. Chem. Ref. Data **38**, 1013 (2009).

[45] P. B. Johnson and R. W. Christy, Phys. Rev. B **9**, 5056 (1974).

[46] C. Schinke, P. C. Peest, J. Schmidt, R. Brendel, K. Bothe, M. R. Vogt, I. Kröger, S. Winter, A. Schirmacher, S. Lim, H. T. Nguyen, and D. MacDonald, AIP Adv. **5**, 067168 (2015).

[47] G. Schütz, S. Stähler, M. Knülle, P. Fischer, S. Parkin, and H. Ebert, J. Appl. Phys. **73**, 6430 (1993).

[48] E. R. Moog, J. Zak, and S. D. Bader, J. Appl. Phys. **69**, 880 (1991).

[49] D. Sander, S. O. Valenzuela, D. Makarov, C. H. Marrows, E. E. Fullerton, P. Fischer, J. McCord, P. Vavassori, S. Mangin, P. Pirro, B. Hillebrands, A. D. Kent, T. Jungwirth, O. Gutfleisch, C.-G. Kim, and A. Berger, J. Phys. D: Appl. Phys. **50**, 363001 (2017).

[50] E. Y. Vedmedenko, R. K. Kawakami, D. D. Sheka, P. Gambardella, A. Kirilyuk, A. Hirohata, C. Binek, O. Chubykalo-Fesenko, S. Sanvito, B. J. Kirby, J. Grollier, K. Everschor-Sitte, T. Kampfrath, C.-Y. You, and A. Berger, J. Phys. D **53**, 453001 (2020).

[51] R. Atkinson and P. H. Lissberger, Appl. Opt. **31**, 6076 (1992).